PHOTONICS Research

Multi-channel multiplexing quantum teleportation based on the entangled sideband modes

Yimiao Wu,[1,†] Qingwei Wang,[1,†] Long Tian,[1,2,†] Xiaoli Zhang,[1] Jiawei Wang,[1] Shaoping Shi,[1] Yajun Wang,[1,2] and Yaohui Zheng[1,2,*]

[1]State Key Laboratory of Quantum Optics and Quantum Optics Devices, Institute of Opto-Electronics, Shanxi University, Taiyuan 030006, China
[2]Collaborative Innovation Center of Extreme Optics, Shanxi University, Taiyuan 030006, China
*Corresponding author: yhzheng@sxu.edu.cn

Received 30 March 2022; revised 7 June 2022; accepted 14 June 2022; posted 16 June 2022 (Doc. ID 459889); published 27 July 2022

Quantum teleportation is a key primitive across a number of quantum information tasks and represents a fundamental ingredient for many quantum technologies. Channel capacity, other than the fidelity, becomes another focus of quantum communication. Here, we present a 5-channel multiplexing continuous-variable quantum teleportation protocol in the optical frequency comb system, exploiting five-order entangled sideband modes. Because of the resonant electro-optical modulation (EOM) that is specifically designed, the fidelities of five channels are greater than 0.78, which are superior to the no-cloning limit of 2/3. This work provides a feasible scheme for implementing efficient quantum information processing.

https://doi.org/10.1364/PRJ.459889

1. INTRODUCTION

Quantum teleportation can transfer to an arbitrary quantum state, including a single-photon state, a vacuum state, a coherent state, and a squeezed state, from one terminal to the other, exploiting shared quantum entanglement and classical communication between two terminals [1–11]. As one of the most basic protocols in quantum information, it serves as a key primitive across a number of quantum information tasks and represents a fundamental ingredient to the development of many quantum technologies, driving the continuing progress of quantum information processing [12–19]. Since the concept of quantum teleportation was proposed in 1993 [1], the fidelity that represents the overlap of the input state and the output state becomes one of the most essential indicators to quantify the teleportation performance [3,20]. Subsequently, the protocol was experimentally demonstrated in optical qubits [21–23], optical modes [3,4,11], atomic ensembles [24,25], trapped atoms [26,27], and solid state systems [28,29]. Thanks to the continuing progress of the entanglement quality, the fidelity of continuous-variable quantum teleportation was gradually increased [30], reaching the maximum value of 0.905 [31].

With the advancement of quantum technology, channel capacity, other than the fidelity, becomes another focus of quantum communication [32]. Channel multiplexing can manifold boost information capacity by integrating several channels into one, which provides a valuable scheme toward effective communication [33,34]. It is well known that many physical systems can support a large number of optical modes to construct many communication channels, such as the orbital angular momentum (OAM) of light [35], the optical frequency comb (OFC) system [36,37], the wavelength-division-multiplexing polarization-entangled photon source [38], and the time-domain multiplexing cluster state [39,40]. Recently, OAM multiplexed quantum teleportation, quantum dense coding, and quantum entanglement swapping have been experimentally implemented [41–43], exploiting the Einstein–Podolsky–Rosen (EPR) entanglement source on OAM superposition modes. For a squeezed field, each pair of symmetric sidebands around the half-pump frequency presents a quantum correlation, which constitutes natural quantum communication channels [37,44]. On the basis of the parametric down-conversion process, the channel multiplexing quantum key distribution based on single-photon entanglement has been demonstrated [38]. Subsequently, we extended the demonstration from the single-photon to the continuous-variable entanglement of optical modes, implementing fourfold channels multiplexing quantum dense coding [45]. However, multi-channel multiplexing quantum teleportation via the OFC system has not yet been demonstrated.

Here, we experimentally demonstrate 5-channel multiplexing quantum teleportation, exploiting five pairs of entangled sideband modes of a single squeezed field. The resonant electro-optical amplitude modulator (EOAM) and the electro-optical phase modulator (EOPM) are specifically designed, addressing the problem of under capacity of the auxiliary beam (Aux). Fivefold entangled sideband modes are spatially separated at the first five resonances of the optical

parametric oscillator (OPO) to perform the quantum teleportation, in turn, corresponding to the fidelity of 0.799, 0.799, 0.791, 0.787, and 0.785, respectively. Since the five quantum channels are located at different resonances of the OPO with large frequency intervals, the cross-talking effect can be completely avoided. By utilizing the OPO with low free spectral range (FSR), the number of the multiplexing channels is expected to scale to a higher level.

2. EXPERIMENT PROCEDUCE

In this protocol of multi-channel multiplexing quantum teleportation, we employ a single broadband squeezed field generated from an OPO as the quantum resource. A squeezed field involves many EPR entangled modes at the symmetric sidebands of $\omega_{\pm i}$ $(i = 1, 2, \ldots, n)$ around the half-pump frequency within the phase-matching bandwidth of the nonlinear crystal [33,45,46]. Each pair of the entangled modes can independently perform the quantum teleportation protocol. The entangled sideband modes are divided into an upper sideband mode (EPR+) and a lower sideband mode (EPR–) by two frequency dependent beam splitters. An unknown input state combines with the EPR+ at a balanced beam splitter (BS), and the output fields are detected by two balanced homodyne detectors (BHDs) to extract the phase and amplitude quadratures information at Alice's station. The detected signals are transmitted to Bob's station through classical channels. The Aux obtains the transmitted information by utilizing an EOAM and an EOPM. The Aux carrying the acquired information is combined with the EPR– at a 1:99 ratio BS to reassemble the initial input state. In order to implement the teleportation process, we generate coherent upper and lower sideband modes with the same frequencies as entangled sideband modes by using a fiber-coupled waveguide electro-optical modulator (WGM). The coherent sideband modes have four functions: the locking beam, the input state, the local oscillators (LOs), and the Aux for classical information extraction. What is worth highlighting is that only one percent of the Aux is reflected to couple with the EPR– to restore the input state during teleportation, which requires a high Aux power to compensate for the coupling loss. However, it is quite less in power in the coherent sideband modes owing to the limited performance of the WGM. To address this problem, we specifically design a resonant EOAM and an EOPM that enhance the modulation depth and reduce the requirement for the Aux power. The output state is then verified by a BHD, and the fidelity is calculated to quantify the teleportation performance.

The detailed experiment setup is shown in Fig. 1. A nonclassical OFC system is generated by pumping a subthreshold OPO. The OPO is a semi-monolithic cavity consisting of a concave mirror driven by piezoceramics and a periodically poled $KTiOPO_4$ (PPKTP) crystal. The threshold power, P_{th}, of the OPO is 220 mW with an FSR, ω_{FSR}, of 3.325 GHz. In the OFC system, a squeezed carrier field has a non-classical noise reduction of 12.6 dB without the electronic noise corrected [47], and the symmetric sideband modes are used as the EPR entangled resources because of the correlated characteristics [44]. However, the entangled sideband modes of the OPO are vacuum states [34]. A locking beam

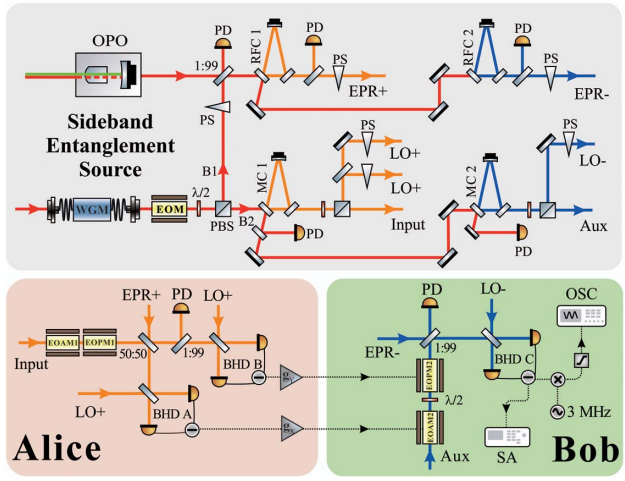

Fig. 1. Schematic of the experimental setup for multi-channel multiplexing quantum teleportation. OPO, optical parameter oscillator; PS, phase shifter; RFC, ring filter cavity; MC, mode cleaner; WGM, waveguide electro-optical modulator; EOAM, electro-optical amplitude modulator; EOPM, electro-optical phase modulator; PBS, polarization beam splitter; $\lambda/2$, half-wave plate; EOM, electro-optical modulator; PD, photo detector; Aux, auxiliary beam; BHD, balanced homodyne detector; LO, local oscillator; SA, spectrum analyzer; and OSC, oscilloscope.

is introduced to manage the downstream ring filter cavities (RFCs) and the BHDs [45,48,49]. The coherent upper and lower sideband modes from the WGM are divided into four parts by utilizing polarization beam splitters (PBS) and mode cleaners (MCs), which serve as the locking beam (B1), the input state, the LOs, and the Aux. The WGM has a modulation bandwidth and insertion loss of 20 GHz and 3 dB, which is driven in turn by a modulation frequency of $n\omega_{FSR}$ $(n = 1,2,3,4,5)$. The signal generator (Keysight E8257D PSG) has a bandwidth and power of 20 GHz and 25 dBm. Therefore, the 1st to 5th coherent sideband modes can be generated to assist the teleportation process.

As shown in Fig. 2(a), the upper and lower sideband modes are resonated with RFC1 and RFC2, respectively. Hence, the RFCs transmit the resonant sideband modes and reflect the rest. In order to reduce the decoherence from the separation process of the upper and lower sideband modes, the RFC as the frequency dependent beam splitter should have the loss as low as possible [50,51]. The influences of the impedance matching, the linewidth, and the sideband suppression ratio of the RFCs on the entanglement degree are synthetically considered in the design and construction of the RFC. The RFC is an impedance-matching cavity with a round-trip length, fineness, and linewidth of 232.0 mm, 29.8, and 43.4 MHz, respectively. Figures 2(b)–2(f) show the mode resolution capabilities of the RFCs for the 1st to the 5th sideband modes, indicating that the lower sideband modes are reflected under the resonance condition of the corresponding upper sideband modes. All results are normalized to the FSR of the OPO. In addition, it is known, from Fig. 2, that the lower sidebands have the reflectivity of 98.5%, 99.5%, 99.7%, 99.7%, and 99.6%, respectively, when the corresponding upper sidebands resonate with

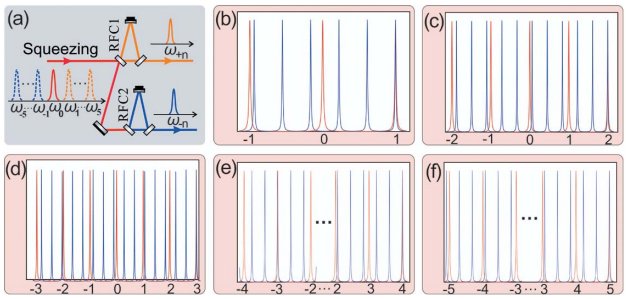

Fig. 2. (a) Schematic of the spatial separation of the entangled sideband modes utilizing the ring filter cavities (RFCs). (b)–(f) The transmission peak for the 1st to the 5th sideband modes. The red lines represent the longitudinal modes of the OPO, and the blue lines represent the longitudinal modes of the RFC. When the upper sideband resonates with the RFC, the lower symmetrical sideband is almost completely reflected.

the RFC. Owing to the limited bandwidth of the BHDs, the residual transmission of the non-resonance sideband modes does not interfere with the teleportation process. The MCs serving as the generation of coherent sideband modes have an extremely low power transmittance (about 0.001%) for the non-resonant sidebands and carrier to avoid interfering with the measurement. All these cavities are actively controlled using the Pound–Drever–Hall technique [52].

In Alice's terminal, the EPR+ beam is coupled with the input state, a_{in}, at a balanced BS, performing a joint measurement with two BHDs by interfering with the LO+. The relative phases of BHDs A and B are locked to 0 and $\pi/2$ to derive the amplitude and phase information of the input state, respectively. The detected amplitude and phase information are transmitted to Bob's station through the classical channels with proper gain. The Aux is used to get the transmitted information utilizing the EOAM2 and the EOPM2. A half-wave plate placed between the EOAM2 and the EOPM2 is precisely adjusted to make sure there is no interference between the amplitude and the phase modulation [4,53]. After modulation, the Aux is coupled with the EPR– at a mirror with the transmissivity of 0.99, and the relative phase between the Aux and the EPR– is locked to 0. The output beam is verified with the BHD C by interfering with the LO-. To reduce the uncertainty in the measurement, the three homemade BHDs are selected to have the same performance and high common mode rejection ratio [54]. The alternating current (AC) output of BHD C is split into two parts via a power splitter. One is measured by a spectrum analyzer to obtain the noise power in the frequency domain. The other is mixed with an electrical signal to get the time-domain signal on an oscilloscope to reconstruct the Wigner function of the teleported state. Finally, we can calculate the fidelity from the noise power and the Wigner function of the output state to verify whether quantum teleportation is successfully implemented.

3. EXPERIMENTAL RESULTS

Before the teleportation process, the correlation noise variances of the first five pairs of the entangled sideband modes of the OPO are measured by utilizing the existing instruments. We add the output signals of BHD A and BHD B to obtain the total noise variance of the upper sideband mode. The noise variance of the lower sideband mode is measured by using the single BHD C, which is combined with the output of BHD A and BHD B to read the correlation noise. The correlation noises of the amplitude sum and the phase difference for the 1st to the 5th entangled sideband modes are unbiased and equal to 6 dB. During the measurement of each order entangled sideband mode, the powers of the LOs are equal and remain unchanged.

For quantum teleportation, the fidelity $F \equiv \langle \psi_{\text{in}} | \rho_{\text{out}} | \psi_{\text{in}} \rangle$ is a crucial indictor of quantifying quantum teleportation, where ψ_{in} represents the input state, and ρ_{out} is the density matrix of output state [3]. In the actual teleported process with the entangled sideband modes, the fidelity of the teleported state is quantified by

$$F = \frac{2}{\sigma_Q} \exp\left(-\frac{2}{\sigma_Q}|\beta_{\text{out}} - \beta_{\text{in}}|^2\right), \tag{1}$$

where

$$\sigma_Q = \sqrt{(1+\sigma_W^x)(1+\sigma_W^p)}, \tag{2}$$

$$\sigma_W^x = \sigma_W^p = g^2 + \frac{1}{2}e^{2r}(1-g)^2 + \frac{1}{2}e^{-2r}(1+g)^2. \tag{3}$$

β_{in} and β_{out} represent the amplitudes of the input and the output states, and σ_Q is the noise variance of the Q function of the output state. σ_W^x and σ_W^p are the noise variances of the amplitude and the phase quadratures of the output state, r ($0 \le r < \infty$) is the squeezing factor, and g is the gain factor of the classical channel, which is selected as the unity value for the amplitude and the phase quadratures [4,55]. To achieve quantum teleportation, the signals detected by Alice must be transmitted to Bob with proper gain and phase shift. The process of regulating the gain is shown in Fig. 3(a). A modulation signal with a modulated frequency and amplitude of 3 MHz and 20 dB is imposed on the input state. Without the EPR state, the noise powers of the amplitude and the phase quadratures detected via Bob's BHD are 20 dB higher than the shot noise limit (SNL) [Traces (iii) and (iv)]. When the modulated signal is turned off, the noise variance of the amplitude and the phase quadrature is 4.77 dB higher than the SNL, and the classical teleportation is confirmed [Trace (ii)]. In addition, the relative phase between the amplitude and the phase quadratures is $\pi/2$.

During the teleportation process, there are multiple phases that need to be controlled. The phase fluctuations originating from nonideal phase locking will reduce the system fidelity. When the phase fluctuations in the phase-locking loops are constant, the phase fluctuation caused by the anti-squeezing quadrature results in the increased additional noise and reduced fidelity [31]. As shown in Fig. 3(b), for the 1st entangled sideband mode, when the pump power is 120 mW, 100 mW, 80 mW, and 60 mW, the corresponding fidelity is 0.751, 0.768, 0.799, and 0.749, respectively. The highest fidelity is 0.799 at the pump power of 80 mW, corresponding to the

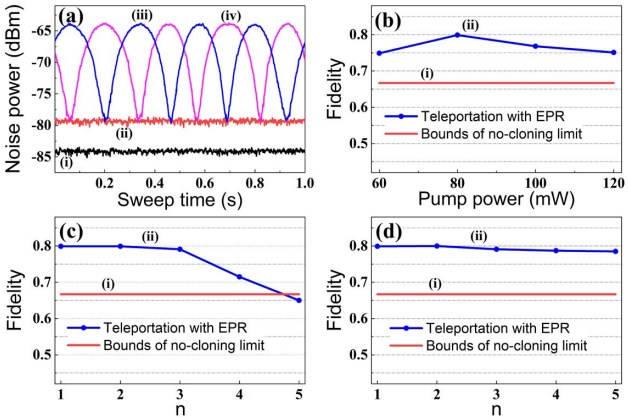

Fig. 3. (a) Noise power recorded by BHD C of a coherent input beam without entanglement to optimize the gain factor. (b) The fidelity at different pump powers with the 1st entangled sideband mode as the quantum resource. (c) The fidelity utilizing the broadband EOAM and the EOPM with the 1st to the 5th sideband entangled modes. (d) The fidelity utilizing the resonant EOAM and the EOPM with the 1st to the 5th sideband entangled modes. n is the order. For (b)–(d), the red lines are the bounds of the no-cloning limit, the blue points are the fidelities of the teleported state under different conditions, and the blue lines are the visual guidance [Trace (ii)].

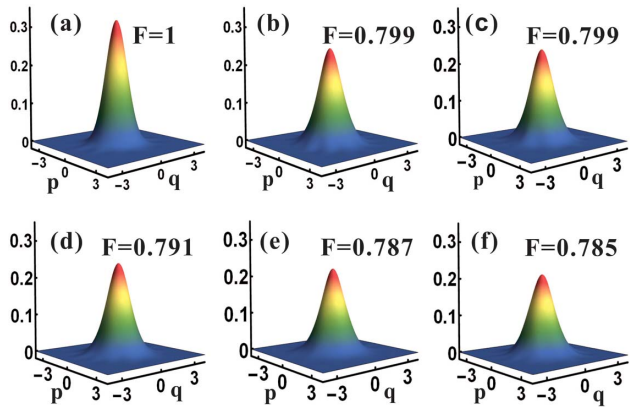

Fig. 4. Reconstructing the Wigner functions of the input and output states. (a) The Wigner function of the input state. (b)–(f) The Wigner functions of the output states for the 1st to the 5th entangled sideband modes. p and q are momentum and position in the phase space, respectively.

pump factor of 0.36. For the 1st to the 5th entangled sideband modes, the experimental setup remains unchanged, so there is the same feature for the system loss and the phase fluctuations. In sequence, we achieve the quantum teleportation with the fidelity of 0.799, 0.791, 0.715, and 0.65, respectively, by utilizing the broadband EOAM and the EOPM at the pump factor of 0.36, exploiting the 2nd to the 5th entangled sideband modes, as shown in Fig. 3(c). The fidelities of the 4th and the 5th channels are less than that of the first three channels. This is due to the lower power of the 4th and the 5th coherent sidebands, which limits the effective displacement of the classical signals (the WGM has a limited input power, and signal generator has a lower output power at high frequency). To address this problem, we try to amplify the classical signals in the classical channels by employing two radio frequency power amplifiers in the series. However, the serial amplification results in excess noise, which destroys the quantum teleportation process. Even more to the point, we specifically design the resonant EOAM and the EOPM with the resonant frequency of 3 MHz as an effective alternative, which not only compensates for the under capacity of the Aux but also solves the problem of excess noise. After optimization, the quantum teleportation of the 4th and the 5th channels is achieved with fidelities of 0.787 and 0.785.

Figure 3(a) shows the calibration results of the gain factor with a coherent state as the input state at an analysis frequency of 3.0 MHz when the entangled beam is blocked [resolution bandwidth (RBW) = 100 kHz, video bandwidth (VBW) = 100 Hz]. All traces are the noise variances recorded by BHD C. Figure 3(b) shows the fidelity as a function of the pump power with the 1st sideband entangled modes as the quantum resource. Figures 3(c) and 3(d) show the fidelity as a function of the order number n of the sideband entangled modes, exploiting the broadband and resonant EOAM and EOPM as the displaced state generating devices, respectively. To obtain the complete quantum characteristics of the output state, the Wigner functions of the input state and teleported states utilizing the resonant EOAM and EOPM are reconstructed as shown in Fig. 4. Figure 4(a) represents the reconstructed Wigner function for the input state, and Figs. 4(b)–4(f) are the reconstructed Wigner functions of the teleported state with the 1st to the 5th entangled sideband modes, respectively. The fidelities of the five channels are greater than 0.78, which are superior to the no-cloning limit of 2/3 [56].

4. CONCLUSION

In summary, we have presented five parallel channels quantum teleportation based on the OFC system. Because of the resonant EOAM and the EOPM, which are specifically designed, we address the problem of under capacity of the Aux with the 4th and the 5th entangled sideband modes as quantum resources. The fidelities of the 1st to the 5th channels are 0.799, 0.799, 0.791, 0.787, and 0.785, respectively, which are superior to the no-cloning limit of 2/3. Due to the limitation of the WGM and signal generator, more higher-order quantum channels are not demonstrated. We expect to scale the number of the multiplexing channels to a higher level by employing a high-power and broadband WGM, a broadband signal generator, and an OPO with a low FSR. Our scheme provides an avenue toward establishing the efficiency of quantum communication and quantum networks.

Funding. National Natural Science Foundation of China (62027821, 11654002, 11874250, 12174234, 62035015); National Key Research and Development Program of China (2020YFC2200402); Key Research and Development Program of Shanxi (201903D111001); Program for Sanjin Scholar of Shanxi Province.

Disclosures. The authors declare no conflicts of interest.

Data Availability. Data underlying the results presented in this paper are not publicly available at this time but may be obtained from the authors upon reasonable request.

†These authors contributed equally to this paper.

REFERENCES

1. C. H. Bennett, G. Brassard, C. Crépeau, R. Jozsa, A. Peres, and W. K. Wootters, "Teleporting an unknown quantum state via dual classical and Einstein-Podolsky-Rosen channels," Phys. Rev. Lett. **70**, 1895–1899 (1993).
2. L. Vaidman, "Teleportation of quantum states," Phys. Rev. A **49**, 1473–1476 (1994).
3. A. Furusawa, J. L. Sørensen, S. L. Braunstein, C. A. Fuchs, H. J. Kimble, and E. S. Polzik, "Unconditional quantum teleportation," Science **282**, 706–709 (1998).
4. T. C. Zhang, K. W. Goh, C. W. Chou, P. Lodahl, and H. J. Kimble, "Quantum teleportation of light beams," Phys. Rev. A **67**, 033802 (2003).
5. S. L. Braunstein and H. J. Kimble, "Teleportation of continuous quantum variables," Phys. Rev. Lett. **80**, 869–872 (1998).
6. N. Takei, T. Aoki, S. Koike, K.-I. Yoshino, K. Wakui, H. Yonezawa, T. Hiraoka, J. Mizuno, M. Takeoka, M. Ban, and A. Furusawa, "Experimental demonstration of quantum teleportation of a squeezed state," Phys. Rev. A **72**, 042304 (2005).
7. S. Pirandola, J. Eisert, C. Weedbrook, A. Furusawa, and S. L. Braunstein, "Advances in quantum teleportation," Nat. Photonics **9**, 641–652 (2015).
8. D. Bouwmeester, J.-W. Pan, K. Mattle, M. Eibl, H. Weinfurter, and A. Zeilinger, "Experimental quantum teleportation," Nature **390**, 575–579 (1997).
9. F. Dell'Anno, S. D. Siena, L. Albano, and F. Illuminati, "Continuous-variable quantum teleportation with non-Gaussian resources," Phys. Rev. A **76**, 022301 (2007).
10. T. C. Ralph, "All-optical quantum teleportation," Opt. Lett. **24**, 348–350 (1999).
11. W. P. Bowen, N. Treps, B. C. Buchler, R. Schnabel, T. C. Ralph, H. A. Bachor, T. Symul, and P. K. Lam, "Experimental investigation of continuous-variable quantum teleportation," Phys. Rev. A **67**, 032302 (2003).
12. H. J. Kimble, "The quantum internet," Nature **453**, 1023–1030 (2008).
13. K. S. Chou, J. Z. Blumoff, C. S. Wang, P. C. Reinhold, C. J. Axline, Y. Y. Gao, L. Frunzio, M. H. Devoret, L. Jiang, and R. J. Schoelkopf, "Deterministic teleportation of a quantum gate between two logical qubits," Nature **561**, 368–373 (2018).
14. A. Furusawa and N. Takei, "Quantum teleportation for continuous variables and related quantum information processing," Phys. Rep. **443**, 97–119 (2007).
15. J. Yoshikawa, Y. Miwa, A. Huck, U. L. Andersen, P. V. Loock, and A. Furusawa, "Demonstration of a quantum nondemolition sum gate," Phys. Rev. Lett. **101**, 250501 (2008).
16. P. V. Loock and S. L. Braunstein, "Multipartite entanglement for continuous variables: a quantum teleportation network," Phys. Rev. Lett. **84**, 3482–3485 (2002).
17. X. Sun, Y. Wang, Y. Tian, Q. Wang, L. Tian, Y. Zheng, and K. Peng, "Deterministic and universal quantum squeezing gate with a teleportation-like protocol," Laser Photon. Rev. **16**, 2100329 (2022).
18. Q. Wang, Y. Wang, X. Sun, Y. Tian, W. Li, L. Tian, X. Yu, J. Zhang, and Y. Zheng, "Controllable continuous variable quantum state distributor," Opt. Lett. **46**, 1844–1847 (2021).
19. Z.-S. Yuan, Y.-A. Chen, B. Zhao, S. Chen, J. Schmiedmayer, and J. W. Pan, "Experimental demonstration of a BDCZ quantum repeater node," Nature **454**, 1098–1101 (2008).
20. U. L. Andersen and T. C. Ralph, "High-fidelity teleportation of continuous-variable quantum states using delocalized single photons," Phys. Rev. Lett. **111**, 050504 (2013).
21. S. Takeda, T. Mizuta, M. Fuwa, P. V. Loock, and A. Furusawa, "Deterministic quantum teleportation of photonic quantum bits by a hybrid technique," Nature **500**, 315–318 (2013).
22. X.-L. Wang, X.-D. Cai, Z.-E. Su, M.-C. Chen, D. Wu, L. Li, N.-L. Liu, C.-Y. Lu, and J.-W. Pan, "Quantum teleportation of multiple degrees of freedom in a single photon," Nature **518**, 516–519 (2015).
23. E. Lombardi, F. Sciarrino, S. Popescu, and F. D. Martini, "Teleportation of a vacuum–one-photon qubit," Phys. Rev. Lett. **88**, 070402 (2002).
24. J. F. Sherson, H. Krauter, R. K. Olsson, B. Julsgaard, K. Hammerer, I. Cirac, and E. S. Polzik, "Quantum teleportation between light and matter," Nature **443**, 557–560 (2006).
25. H. Krauter, D. Salart, C. A. Muschik, J. M. Petersen, H. Shen, T. Fernholz, and E. S. Polzik, "Deterministic quantum teleportation between distant atomic objects," Nat. Phys. **9**, 400–404 (2013).
26. M. Riebe, H. Häffner, C. F. Roos, W. Hänsel, J. Benhelm, G. P. T. Lancaster, T. W. Körber, C. Becher, F. Schmidt-Kaler, D. F. V. James, and R. Blatt, "Deterministic quantum teleportation with atoms," Nature **429**, 734–737 (2004).
27. S. Olmschenk, D. N. Matsukevich, P. Maunz, D. Hayes, L.-M. Duan, and C. Monroe, "Quantum teleportation between distant matter qubits," Science **323**, 486–489 (2009).
28. L. Steffen, Y. Salathe, M. Oppliger, P. Kurpiers, M. Baur, C. Lang, C. Eichler, G. Puebla-Hellmann, A. Fedorov, and A. Wallraff, "Deterministic quantum teleportation with feed-forward in a solid state system," Nature **500**, 319–322 (2013).
29. W. Pfaff, B. J. Hensen, H. Bernien, S. B. V. Dam, M. S. Blok, T. H. Taminiau, M. J. Tiggelman, R. N. Schouten, M. Markham, D. J. Twitchen, and R. Hanson, "Unconditional quantum teleportation between distant solid-state quantum bits," Science **345**, 532–535 (2014).
30. M. Yukawa, H. Benichi, and A. Furusawa, "High-fidelity continuous-variable quantum teleportation toward multistep quantum operations," Phys. Rev. A **77**, 022314 (2008).
31. Q. Wang, Y. Tian, W. Li, L. Tian, Y. Wang, and Y. Zheng, "High-fidelity quantum teleportation toward cubic phase gates beyond the no-cloning limit," Phys. Rev. A **103**, 062421 (2021).
32. M. V. Larsen, X. Guo, C. R. Breum, J. S. Neergaard-Nielsen, and U. L. Andersen, "Fiber-coupled EPR-state generation using a single temporally multiplexed squeezed light source," npj Quantum Inf. **5**, 46 (2019).
33. M. Heurs, J. G. Webb, A. E. Dunlop, C. C. Harb, T. C. Ralph, and E. H. Huntington, "Multiplexed communication over a high-speed quantum channel," Phys. Rev. A **81**, 856–858 (2010).
34. B. Hage, A. Samblowski, and R. Schnabel, "Towards Einstein-Podolsky-Rosen quantum channel multiplexing," Phys. Rev. A **81**, 062301 (2010).
35. N. Bozinovic, Y. Yue, Y. Ren, M. Tue, P. Kristensen, H. Huang, A. E. Willner, and S. Ramachandran, "Terabit-scale orbital angular momentum mode division multiplexing in fibers," Science **340**, 1545–1548 (2013).
36. H. Song, H. Yonezawa, K. B. Kuntz, M. Heurs, and E. H. Huntington, "Quantum teleportation in space and frequency using entangled pairs of photons from a frequency comb," Phys. Rev. A **90**, 042337 (2014).
37. J. Roslund, R. M. de Araújo, S. Jiang, C. Fabre, and N. Treps, "Wavelength-multiplexed quantum networks with ultrafast frequency combs," Nat. Photonics **8**, 109–112 (2014).
38. S. Wengerowsky, S. K. Joshi, F. Steinlechner, H. Hübel, and R. Ursin, "An entanglement-based wavelength-multiplexed quantum communication network," Nature **564**, 225–228 (2018).
39. M. V. Larsen, X. Guo, C. R. Breum, J. S. Neergaard-Nielsen, and U. L. Andersen, "Deterministic generation of a two-dimensional cluster state," Science **366**, 369–372 (2019).
40. N. C. Menicucci, P. V. Loock, M. Gu, C. Weedbrrook, T. C. Ralph, and M. A. Nielsen, "Universal quantum computation with continuous-variable cluster states," Phys. Rev. Lett. **97**, 110501 (2006).
41. S. Liu, Y. Lou, and J. Jing, "Orbital angular momentum multiplexed deterministic all-optical quantum teleportation," Nat. Commun. **11**, 3875 (2020).
42. Y. Chen, S. Liu, Y. Lou, and J. Jing, "Orbital angular momentum multiplexed quantum dense coding," Phys. Rev. Lett. **127**, 093601 (2021).
43. S. Liu, Y. Lou, Y. Chen, and J. Jing, "All-optical entanglement swapping," Phys. Rev. Lett. **128**, 060503 (2022).
44. J. Zhang, "Einstein-Podolsky-Rosen sideband entanglement in broadband squeezed light," Phys. Rev. A **67**, 054302 (2003).

45. S. Shi, L. Tian, Y. Wang, Y. Zheng, C. Xie, and K. Peng, "Demonstration of channel multiplexing quantum communication exploiting entangled sideband modes," Phys. Rev. Lett. **125**, 070502 (2020).
46. M. Chen, N. C. Menicucci, and O. Pfister, "Experimental realization of multipartite entanglement of 60 modes of a quantum optical frequency comb," Phys. Rev. Lett. **112**, 120505 (2014).
47. W. Yang, S. Shi, Y. Wang, W. Ma, Y. Zheng, and K. Peng, "Detection of stably bright squeezed light with the quantum noise reduction of 12.6 dB by mutually compensating the phase fluctuations," Opt. Lett. **42**, 4553–4556 (2017).
48. L. Tian, S.-P. Shi, Y.-H. Tian, Y.-H. Wang, Y. Zheng, and K.-C. Peng, "Resource reduction for simultaneous generation of two types of continuous variable nonclassical states," Front. Phys. **16**, 21502 (2021).
49. H. Vahlbruch, S. Chelkowski, B. Hage, A. Franzen, K. Danzmann, and R. Schnabel, "Coherent control of vacuum squeezing in the gravitational-wave detection band," Phys. Rev. Lett. **97**, 011101 (2006).
50. P. Barriga, C. Zhao, and D. G. Blair, "Optical design of a high power mode-cleaner for AIGO," Gen. Relativ. Gravit. **37**, 1609–1619 (2005).
51. E. H. Huntington and T. C. Ralph, "Separating the quantum sidebands of an optical field," J. Opt. B **4**, 123–128 (2002).
52. E. D. Black, "An introduction to Pound–Drever–Hall laser frequency stabilization," Am. J. Phys. **69**, 79–87 (2001).
53. M. Huo, J. Qin, J. Cheng, Z. Yan, Z. Qin, X. Su, X. Jia, C. Xie, and K. Peng, "Deterministic quantum teleportation through fiber channels," Sci. Adv. **4**, 9401 (2018).
54. J.-R. Wang, Q.-W. Wang, L. Tian, J. Su, and Y.-H. Zheng, "A low-noise, high-SNR balanced homodyne detector for the bright squeezed state measurement in 1–100 kHz range," Chin. Phys. B **29**, 034205 (2020).
55. S. L. Braunstein, C. A. Fuchs, H. J. Kimble, and P. V. Loock, "Quantum versus classical domains for teleportation with continuous variables," Phys. Rev. A **64**, 022321 (2001).
56. W. K. Wootters and W. H. Zurek, "A single quantum cannot be cloned," Nature **299**, 802–803 (1982).